[1]*Asmaa Guendouz
[2]Mustapha Hatti
[3]Abdelhalim Tlemçani
[4]Hind Saidani-Scott

Longitudinal Control of Autonomous Electric Vehicles via Genetic Algorithm tuned PID and Lyapunov-based Adaptive Control: A Robustness Evaluation Under Dynamic Uncertainties

JES Journal of Electrical Systems

Abstract: - The proposed work consists in a significant contribution to the field of motion planning and control of autonomous electric vehicles. Sinusoidal and S-curve speed profiles are developed and discussed to enable smooth transitions while minimizing jerks that could affect vehicle stability and passenger comfort. These assessments build a foundation for longitudinal control. A conventional PID controller is first implemented to achieve basic speed tracking performance. While it performs adequately, it demonstrates notable limitations. To enhance this latter, the PID gains are optimized using a metaheuristic optimization technique based on Genetic Algorithms (GA). This approach automatically tunes the controller parameters, resulting in improved dynamic response and reduced tracking errors. However, due to their fixed-parameter structure, both classical and optimized PID controllers encounter difficulties in adapting to system variations. To overcome these challenges, Lyapunov-based Model Reference Adaptive Control (MRAC) mechanism is cautiously designed to dynamically adjust the system parameters, compensating for the uncertainties, disturbances, and non-linearities under which real vehicles inherently operate under. Simulation results are finally conducted to validate the proposed control system.

Keywords: Autonomous vehicles, Lyapunov-based Adaptive control, Genetic Algorithms, Speed profiling.

I. INTRODUCTION

Electric Autonomous vehicles (EAVs) are a significant research focus within the automotive field, holding a promise to enhance road safety, improve traffic efficiency, and offer human comfort [1]. Considerable research has been conducted and evolved from the early successful implementations in the 1980s by the pioneer institutions in autonomous vehicle, Carnegie Mellon University to the present day, addressing a wide array of topics, such as vehicle dynamics, energy efficiency, sensor integration, control systems, system reliability [2],[3] and Motion planning. In particular, speed profiling is one of the most important modules in Motion planning [4]. Many scholars have carried out related research in response to the above subject. This paper proposes a contribution in addition to the significant advancements in this field, introducing the S-curve and Sinusoidal profiles [5]. Firstly, an algorithm is built for the profile calculation following the constraints of comfort and road standards. Next, a comparative study is conducted to select an optimal speed profile that ensures safety, efficiency, and passenger comfort. In order to achieve the above selection, a traditional PID longitudinal control system is initially established. To further enhance performance, this Latter is optimized using Genetic Algorithm (GA) based metaheuristic tuning methods [6]. Genetic Algorithms provide global search capabilities, making them a powerful tool for optimizing PID controller gains by searching for the combination that yields the best system performance according to a predefined objective function, the Integral of Squared Error in this case. However, the system remains vulnerable to variations and external uncertainties, conditions under which both classical and optimized PID controllers struggle due to their fixed-parameter configuration. Model Reference Adaptive Control approach is subsequently introduced, to establish a robust theoretical foundation using Lyapunov's method to ensure the stability of the closed-loop system [7]. This study aims to highlight that PID controller's fixed configuration makes them limited in the presence of parameter variations and system uncertainties, despite the improvements provided by the advanced metaheuristic optimization methods. In such cases, adaptive control methods, particularly those

[1]* PhD Student, Electrical Engineering and Automation Research Laboratory (LREA), University of Medea, Medea, Algeria. guendouz.asma@univ-medea.dz.
[2] Doctor, UDES, Unité de Développement des Equipements Solaires, BP 386, 42004 Bou Ismail, Tipaza, Algeria. mustapha.hatti@ieee.org
[3] Professor, Electrical Engineering and Automation Research Laboratory (LREA), University of Medea, Medea, Algeria. tlemcani.abdelhalim@univ-medea.dz
[4] Doctor, Mechanical Engineering Department, University of Bristol, United Kingdom. h.saidani@bristol.ac.uk

based on Lyapunov stability theory, continue to provide superior robustness and consistent performance, reaffirming their relevance for systems with dynamic characteristics. The configuration of this paper is arranged as follows. The vehicle model is presented in section 2. Section 3 discusses S-curve and Sinusoidal profiles. In section 4, the PID controller design is introduced followed by the GA optimization method. The proposed longitudinal MRAC is detailed in section 5. Finally, simulation results for the performed tests are given to validate the proposed methods. MATLAB is used for modelling and simulation.

II. VEHICLE MODELLING

The kinematic bicycle model is used for modelling the motion of the vehicle, where both front and rear wheels are lumped into one wheel located at the center of the vehicle's rear axis as shown in Fig1 [8], this study assumes negligible side slip and front-wheel-only steering control.

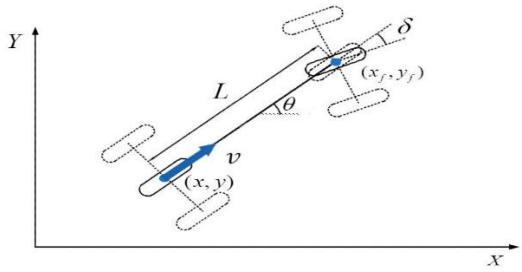

Fig1 Kinematic bicycle model

The nonlinear simplified model is as follows [9]:

$$\dot{x} = v\cos\theta \tag{1}$$

$$\dot{y} = v\sin\theta \tag{2}$$

$$\dot{\theta} = \frac{v\tan\delta}{L} \tag{3}$$

Where x and y represent the vehicle's position, v is the longitudinal velocity, δ is the steering angle, L is the wheelbase and θ is the yaw angle. The model's diagram in Simulink is given below in Fig2.

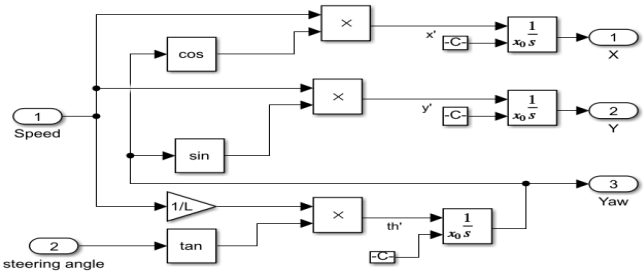

Fig2 Kinematic bicycle model's representation Diagram

III. SPEED PROFILING

In this section, a comparative study between the S-curve profile, including all its variations, and the sinusoidal profile is led, aiming for the most optimized and suited speed in terms of time efficiency, comfort and safety, using equations developed by [5].

A. S–Curve Profile

The function used for this part is a piecewise construct that generalizes all types of S-curve family of profiles. For the generalization, a dimensionless parameter is introduced, denoted γ, varying from 0 to 1, enabling the profile selection. The initialization sequence is given below in Table 1.

Table 1 Parameters initialization for the S-curve profile

Parameter	Symbol	Initialization Formula
Midpoint position	Q_s	$Q_s = \frac{D}{2}$
Auxiliary position	Q_{aux}	$Q_{aux} = \frac{(1+\gamma)}{2} \cdot \left(\frac{{V_m}^2}{A_m}\right)$
Adjusted position	Q_a	$Q_a = \begin{cases} Q_s, & Q_s \le Q_{aux} \\ Q_{aux}, & Q_s > Q_{aux} \end{cases}$
Effective velocity	V_w	$V_w = \begin{cases} \sqrt{\frac{Q_s . A_m}{1/2\,(1+\gamma)}}, & Q_s \le Q_{aux} \\ V_m, & Q_s > Q_{aux} \end{cases}$
Auxiliary constant	T_o	$T_o = \frac{V_m}{A_m}$
Transition time	T_a	$T_a = T_o \cdot (1+\gamma)$
Intermediate time	T_m	$T_m = \frac{T_a}{2}$
Time constant	τ	$\tau = \gamma \cdot T_o$
Constant velocity period	T_k	$T_k = 2 \cdot \frac{Q_s - Q_a}{V_m}$
Midpoint time	T_s	$T_s = T_a + \frac{T_k}{2}$
Total time	T_t	$T_t = 2 \cdot T_s$

The key parameters are: V_m the maximum speed, A_m the maximum acceleration and D the total travelled distance.The position $q(t)$, speed $v(t)$ and acceleration $a(t)$ are defined as:

$$q(t) = \begin{cases} 0, & t \le 0 \\ \left(\frac{1}{2} \cdot \frac{V_w}{T_o}\right) \cdot \left(\frac{t^3}{3 \cdot \tau}\right), & 0 < t < \tau \\ \left(\frac{1}{2} \cdot \frac{V_w}{T_o}\right) \cdot \left[\left(t - \frac{\tau}{2}\right)^2 + \frac{\tau^2}{12}\right], & \tau < t \le T_o \\ Q_s + V_w \cdot (t - T_s) + q(T_a - t), & \tau < t \le T_o \\ Q_f - q(T_t - t), & T_s < t \end{cases} \tag{4}$$

$$v(t) = \begin{cases} 0, & t \le 0 \\ \left(\frac{A_m}{2}\right) \cdot \left(\frac{t^2}{\tau}\right), & 0 < t < \tau \\ \left(\frac{A_m}{2}\right) \cdot (2 \cdot t - \tau), & \tau < t \le T_o \\ V_w - v(T_a - t), & T_m < t \le T_s \\ v(T_t - t), & T_s < t \end{cases} \tag{5}$$

$$a(t) = \begin{cases} 0, & t \le 0 \\ \left(\frac{A_m}{\tau}\right) \cdot t, & 0 < t < \tau \\ A_m, & \tau < t \le T_o \\ a(T_a - t), & T_m < t \le T_s \\ -a(T_t - t), & T_s < t \end{cases} \tag{6}$$

The derived Jerk (change in acceleration) is as follows:

$$j(t) = \begin{cases} 0\ , & t \le 0 \\ J_m, & 0 < t < \tau \\ 0, & \tau < t \le T_o \\ -j(T_a - t), & T_m < t \le T_s \\ j(T_t - t), & T_s < t \end{cases} \quad (7)$$

Where J_m is the jerk limit, an optimized value that ensures comfort and smooth changes in acceleration.

A simulation is conducted to evaluate the performance of the S-curve profile for different values of γ, over a road segment of length *D=2km* where the speed limit is set to 28.8 km/h (8m/s), suitable for urban environments as per the standard ISO 22737. The chosen range for the acceleration limit based on ISO 2631, is 0.315 to 0.63 (m/s^2) (a little uncomfortable). Considering urban travel whilst maintaining safety, smooth driving and passenger comfort is set at 0.4 (m/s^2). **Error! Reference source not found.** presents the S-curve profiles for position, speed, acceleration, and jerk. The plots are segmented according to γ intervals. For $\gamma = 0$, the results present a 3-segment profile also known as the trapezoidal profile, where the velocity increases linearly until it reaches the maximum value $V_w = 8m/s$ that remains constant for $T_k = 229{,}6s$ and then decreases linearly to zero. Meanwhile the acceleration plot remains constant in the acceleration and deceleration phases and null in between, these instantaneous changes, leading to an infinite jerk. Furthermore, the position plot confirms that as γ decreases, the travel time decreases offering a fast response. For $0 < \gamma \le 1$, a 7-segment profile (S-curve profile) is introduced. The acceleration slope is reduced from being a vertical line, which results in a finite jerk leading to a smooth velocity curve with no sharp corners. From **Error! Reference source not found.** it is easy to notice that as γ increases, jerk value decreases which leads to smoother transitions.

Table 2 Comparative table for S-curve parameters

γ	0.25	0.5	0.75	1
$J_m\ (m/s^2)$	0.08	0.04	0.0267	0.02
T_a(s)	25	30	35	40
T_t(s)	275	280	285	290

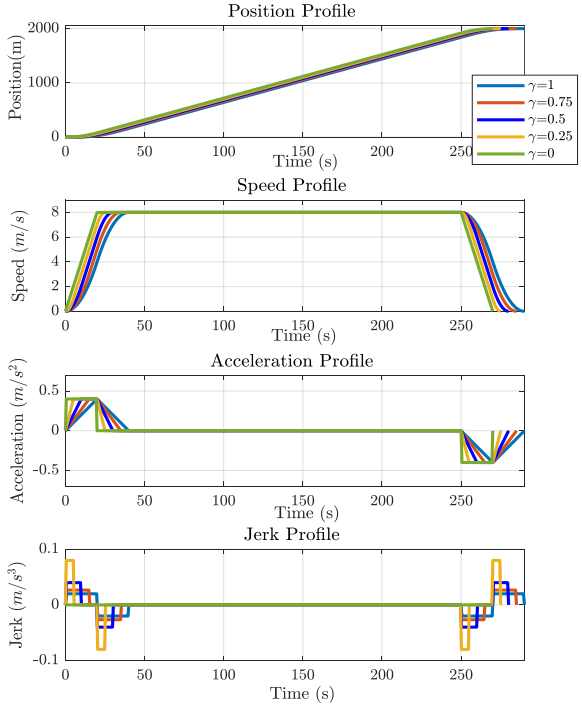

Fig3 S-curve profiles

In summary, although the trapezoidal profile is simple and fast, its sudden changes, abrupt transitions, and high jerk make it unsuitable for ensuring safe and comfortable motion. Therefore, S-curve profiles with higher smoothness are more suitable for autonomous vehicles.

B. Sinusoidal Profile

The initialization sequence for this profile is given in Table 3. Q_s, Q_a, T_o, T_k, T_s and T_t remain unchanged from Table 1.

Table 3 Parameters initialization for the Sinusoidal Profile

Parameter	Initialization
Auxiliary position Q_{aux}	$Q_{aux} = \left(\frac{{V_m}^2}{A_m}\right)$
Effective Velocity V_w	$V_w = \begin{cases} \sqrt{Q_s \cdot A_m}, & Q_s \le Q_{aux} \\ V_m, & Q_s > Q_{aux} \end{cases}$
Transition time T_a	$T_a = 2 \cdot T_o$
Angular frequency ω	$\omega = \frac{2\pi}{T_a}$
Scaling constant K_s	$K_s = \frac{T_a \cdot V_w}{4\pi^2}$

The position $q(t)$, speed $v(t)$ and acceleration $a(t)$ are given by:

$$q(t) = \begin{cases} 0, & t \le 0 \\ \frac{A_m}{4} \cdot t^2 + K_s \cdot (cos(\omega \cdot t) - 1), & 0 < t \le T_a \\ Q_s + V_w \cdot (t - T_s), & T_a < t \le T_s \\ D - q(T_t - t), & t > T_s \end{cases} \tag{8}$$

$$v(t) = \begin{cases} 0, & t \le 0 \\ K_s \cdot \omega \cdot (\omega \cdot t - \sin(\omega . t)), & 0 < t \le T_a \\ V_w & T_a < t \le T_s \\ v(T_t - t), & t > T_s \end{cases} \tag{9}$$

$$a(t) = \begin{cases} 0, & t \le 0 \\ \frac{A_m}{2} \cdot (1 - \cos(\omega . t)), & 0 < t \le T_a \\ 0, & T_a < t \le T_s \\ -a(T_t - t), & t > T_s \end{cases} \tag{10}$$

The jerk is similarly obtained:

$$j(t) = \begin{cases} 0, & t \le 0 \\ \frac{A_m}{2} \cdot (\omega \cdot \sin(\omega . t)), & 0 < t \le T_a \\ 0, & T_a < t \le T_s \\ j(T_t - t), & t > T_s \end{cases} \tag{11}$$

Fig4 shows the results of a comparative study between sinusoidal profile and S-curve profile with $\gamma = 0.5$, keeping the previous scenario with $D = 2km$, $V_m = 8m/s$ and $A_m = 0.4\ m/s^2$. It is observed that the velocity response for both methods offer smooth transitions. However, the total transition time for the S-curve profile is at $T_a = 30s$, while the total transition time for the sinusoidal profile is $T_a = 40s$, causing a slower response. The S-curve acceleration profile changes linearly, taking a trapezoidal form. Moreover, the jerk experiences abrupt changes that cause minor discontinuities whereas the sinusoidal profile maintains a continuous jerk with minimal harmonic content.

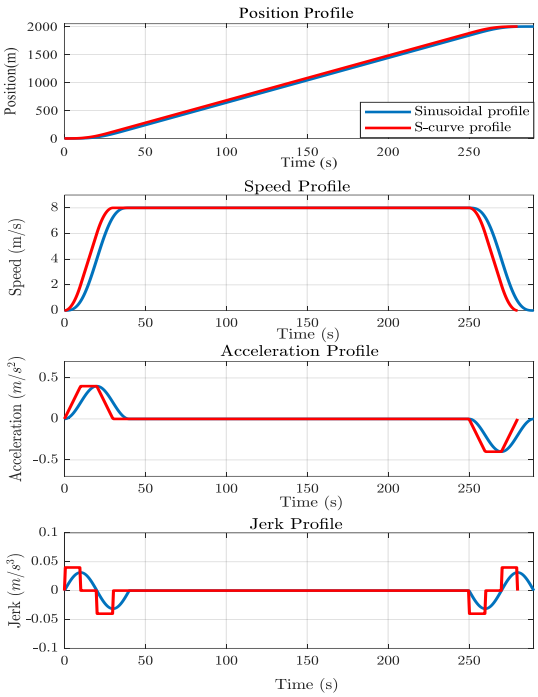

Overall, the S-curve profile offers a good balance between smoothness and computational efficiency despite the slightly reduced comfort caused by the jerk's discontinuities. In contrast, the Sinusoidal profile allows for the smoothest transitions in both acceleration and jerk, resulting in the most refined motion profile; However, it requires more computational power.

Fig1 Sinusoidal and S-curve profiles

IV. CONTROLLER DESIGN

A. Longitudinal control

For the velocity control, the actuator used is a DC motor, described by (12-15) given below [10].

$$V = R_a \cdot i_a + e + L_a \cdot \frac{di_a}{dt} \tag{12}$$

$$e = k \cdot \Omega \tag{13}$$

$$J \cdot \frac{d\Omega}{dt} = T_{em} - f \cdot \Omega - T_L \tag{14}$$

$$T_{em} = k_{em} \cdot i_a \tag{15}$$

Where V is the input voltage, e the back electromotive force (EMF), i_a the current in the motor winding, T_{em}, the electromagnetic torque; and Ω is the angular velocity. The parameters are chosen, based on a similarity with Tesla model S of torque $T_L = 430Nm$, taken from [11]- See Table 4 below.

Table 4 DC Motor Parameters

Parameter	value
Armature resistance R_a	0.193 Ω
Armature inductance L_a	0.00383 H
Back EMF constant k	2.332232 $V \cdot s$
Torque constant k_{em}	2.1717 $N \cdot m/A$
Moment of inertia J	0.6 $kg \cdot m^2$
Coefficient of friction f	2.632177 $N \cdot m \cdot s$

A PID controller is used for the velocity control system, where the following gain terms are adjusted through trial and error to achieve a suitable response: $\boldsymbol{K_p = 19}$, $\boldsymbol{K_i = 100}$, $\boldsymbol{K_D = 0.5}$.

Fig5 illustrates the speed response of the PID control system. The speed reference in this case is the previously discussed sinusoidal velocity profile. It is observed that the suggested controller shows a good stability and tracking performance. However, a noticeable delay is present which can significantly affect the performance, safety, and efficiency of an autonomous vehicle.

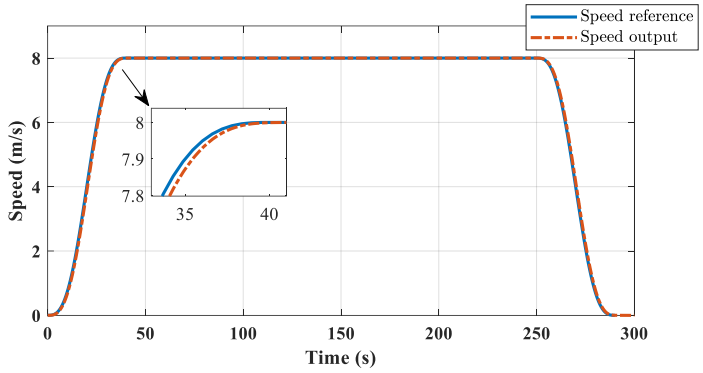

Fig5 Simulation result for the speed control system

B. Genetic Algorithm based PID Optimization

In order to address the observed delay in the previous section, a Genetic Algorithm is employed to optimize the PID gains. GA is an evolutionary metaheuristic algorithm grounded in population dynamics and inspired by the concepts of natural selection and evolutionary processes. It progressively improves potential solutions through selection, crossover, and mutation, ultimately converging on optimal parameters [12]. The code implemented in this study returns the optimal PID gains that minimize a cost function. It evolves a population of 100 solutions over 50 generations, applying crossover (80%) and adaptive feasible mutation. The ISE (Integral of Squared Error) criterion is selected as the objective function. This choice prioritizes reducing tracking errors while minimizing the effect of delays. The operational flowchart of the genetic algorithm utilized in this study is depicted in Fig6.

$$ISE = \int e^2(t)dt \tag{16}$$

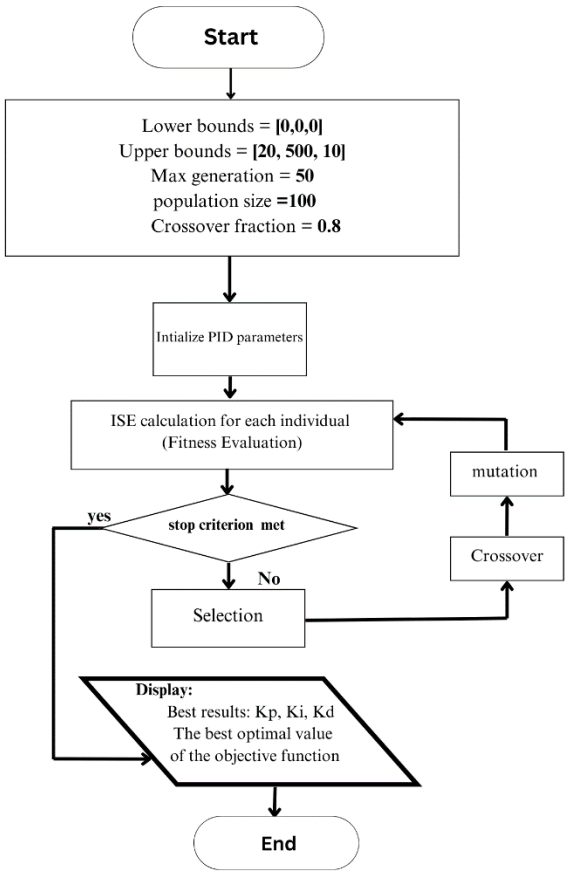

Fig6 Genetic algorithm PID tuning flowchart

Table 5 presents the statistical indices of the algorithm's outcome during the tuning process. The algorithm demonstrates consistent convergence, with the best fitness value improving rapidly in the early generations from 13 onward. The resulting PID parameters:

$K_p = 19.9595, K_i = 499.9999, and\ K_d = 0.1158$, with a **minimum fitness value** of **0.001777**. The gradual reduction in the mean fitness values alongside the stagnation in the best fitness value in later generations indicates the population's convergence towards an optimal region. The increasing stall count also suggests that the GA was reaching a state of exploration-exploitation balance, stabilizing around a high-quality solution.

Table 5 Progress of the Genetic Algorithm.

Generation	Func-count	Best f(x)	Mean f(x)	Stall Generations
1	200	0.001784	1.422	0
2	295	0.001784	0.01696	0
3	390	0.001784	0.005337	1
4	485	0.00178	0.004413	0
5	580	0.00178	0.002221	1
6	675	0.00178	0.002059	0
7	770	0.00178	0.001975	1
8	865	0.00178	0.001789	2
9	960	0.001779	0.001784	0
10	1055	0.001779	0.001782	0
11	1150	0.001779	0.001781	1
12	1245	0.001779	0.00178	2
13	1340	0.001778	0.001779	0
14	1435	0.001778	0.001779	0
15	1530	0.001778	0.001779	0
16	1625	0.001778	0.001779	1
17	1720	0.001778	0.001779	2
18	1815	0.001778	0.001778	0
19	1910	0.001778	0.001778	0
20	2005	0.001778	0.001779	1
21	2100	0.001778	0.001779	2
22	2195	0.001778	0.001778	3
23	2290	0.001777	0.001778	0
24	2385	0.001777	0.001778	0
25	2480	0.001777	0.001778	1
26	2575	0.001777	0.001778	0
27	2670	0.001777	0.001778	1
28	2765	0.001777	0.001778	2
29	2860	0.001777	0.001778	0
30	2955	0.001777	0.001778	0
31	3050	0.001777	0.001778	1
32	3145	0.001777	0.001778	2
33	3240	0.001777	0.001778	3
34	3335	0.001777	0.001778	0
35	3430	0.001777	0.001778	0
36	3525	0.001777	0.001778	0
37	3620	0.001777	0.001778	1
38	3715	0.001777	0.001778	2
39	3810	0.001777	0.001778	3
40	3905	0.001777	0.001777	0
41	4000	0.001777	0.001778	1
42	4095	0.001777	0.001777	0
43	4190	0.001777	0.001777	0
44	4285	0.001777	0.001777	1
45	4380	0.001777	0.001777	2
46	4475	0.001777	0.001777	3
47	4570	0.001777	0.001777	0
48	4665	0.001777	0.001777	1
49	4760	0.001777	0.001777	2
50	4855	0.001777	0.001777	0

Fig7 illustrates the speed response of the control system under: a conventionally tuned PID controller and a Genetic Algorithm (GA)-tuned PID. Both simulations were conducted under identical conditions. The primary observation is the elimination of the

delay that was previously discussed in the earlier section. demonstrating a faster system reaction by the speed response of the GA tuned PID. To further validate these findings, Fig8 depicts the speed error trajectories for both controllers. The overshoot observed in the conventional PID response is **0.04**, indicating that the system initially exceeded the setpoint by **4%**. After applying the GA-based optimization, the overshoot is reduced to **0.0075**, corresponding to a **reduction in overshoot of 81.25%**. This substantial improvement demonstrates the ability of the GA to fine-tune the PID parameters, significantly enhancing system stability and reducing transient errors.

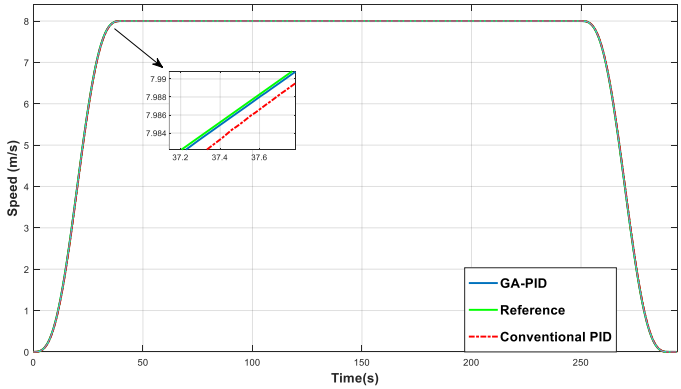

Fig7 Speed response

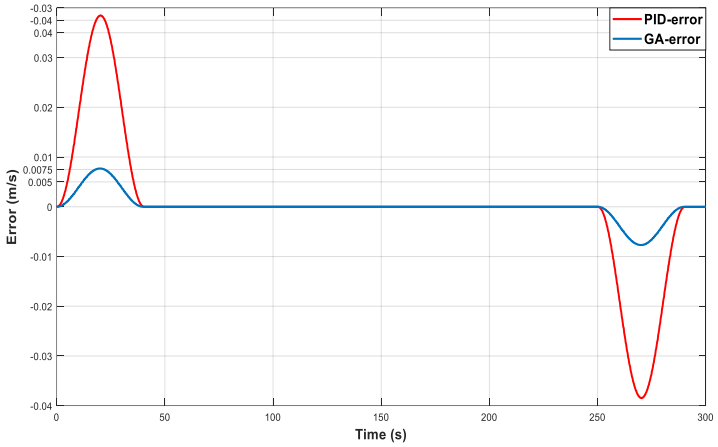

Fig8 Speed Error plot

V. LYAPUNOV-BASED MODEL REFERENCE ADAPTIVE CONTROL

After the evaluation of the performance enhancements achieved through Genetic Algorithm-based PID tuning, it is important to consider dynamics uncertainties. In such cases, fixed-parameter controllers may not provide. Which leads to the exploration of Lyapunov-based MRAC, a commonly employed control strategy enabling a system to follow a desired reference model despite uncertainties and variations. It uses Lyapunov's stability theory to construct the adjustment mechanism [13],[14],[15].

Considering the main system with the output denoted by y and the reference model with the output denoted by y_c as described by (17) and (18) respectively, where $a_i(t)$ and $K_s(t)$ are time-varying coefficients, b_j and K_m are the model's constant coefficients and y_c is the desired input.

$$y^{(N)} + \sum_{i=0}^{N-1} a_i(t) y^{(i)} = K_s(t) y_c(t) \tag{17}$$

$$y_m^{(N)} + \sum_{j=0}^{N-1} b_j y_m^{(j)} = K_m y_c(t) \tag{18}$$

The tracking error is defined as follows:

$$e^{(i)} = y_m^{(i)} - y^{(i)} \tag{19}$$

To achieve zero error, the parameters are adjusted within a time interval $t \in [t_n, t_n + T_n]$ according to the following criteria:

$$\begin{array}{rcl} k_s(t) & = & k_a(t)k_0(t) = k_a(t)k_0(T_n) \\ a_i(t) & = & a_i(T_n) + k_0(T_n)c_i(t) \end{array} \tag{20}$$

$k_a(t)$ is the controller gain, $k_0(t)$ and $c_i(t)$ are adjusted parameters.

By defining the adjustable parameters denoted γ_i as follows:

$$\begin{array}{rcl} \gamma_{n+1} & = & k_m - k_a(t)k_0(T_k) \\ \gamma_n & = & b_{n-1} - [a_{n-1}(T_k) + k_0(T_k)c_{n-1}] \\ \ldots & \ldots & \ldots \\ \gamma_1 & = & b_0 - [a_0(T_k) + k_0(T_k)c_0] \end{array} \tag{21}$$

The control law can be written in the following way:

$$\begin{array}{c} u_0(t) = \gamma_{n+1}y_c(t) - \gamma_n y^{(n-1)} - \gamma_{n-1}y^{(n-2)} \\ - \cdots - \gamma_1 y \end{array} \tag{22}$$

Given: $e^{(i)} = x_{i+1}$, a system of equations is obtained, see (23). The condensed form of the latter is given in (24).

$$\begin{array}{rcl} \dot{x}_1 & = & x_2, \\ \dot{x}_2 & = & x_3, \\ \ldots & : & : \\ \dot{x}_{n-1} & = & x_n, \\ \dot{x}_n & = & -b_0x_1 - b_1x_2 - \cdots - b_{n-1}x_n + u_0(t); \end{array} \tag{23}$$

$$\dot{x} = Ax + u \tag{24}$$

Where:

$$A = \begin{bmatrix} 0 & 1 & 0 & \ldots & 0 \\ 0 & 0 & 1 & \ldots & 0 \\ \ldots & \ldots & \ldots & \ldots & 0 \\ \vdots & \ldots & \ldots & \ldots & 1 \\ -b_0 & -b_1 & -b_2 & \ldots & -b_{n-1} \end{bmatrix}; u = \begin{bmatrix} 0 \\ 0 \\ \vdots \\ u_0 \end{bmatrix} \tag{25}$$

The positive-definite Lyapunov function in (26) is chosen based on the concept of energy that satisfies the negative (semi-) definiteness of its time derivative.

$$V = x^T P x + \sum_{i=1}^{n+1} \lambda_i \gamma_i^2 \tag{26}$$

λ_i are positive weighting constants and P is a positive definite symmetric matrix.

$$P = \begin{bmatrix} p_{11} & p_{12} & \ldots & p_{1n} \\ p_{21} & p_{22} & \ldots & p_{2n} \\ \ldots & \ldots & \ldots & \ldots \\ p_{n1} & p_{n2} & \ldots & p_{nn} \end{bmatrix} \tag{27}$$

Using (24) and assuming that the matrix A is regular, the time derivative of V is obtained by:

$$\dot{V} = x^T(A^T P + PA)x + 2x^T P u + \sum_{i=1}^{n+1} 2\lambda_i \gamma_i \dot{\gamma}_i \tag{28}$$

Given $A^T P + PA = -Q$, where Q is a diagonal matrix with elements $q_{ij} > 0$.

$$Q = \begin{bmatrix} q_{11} & 0 & \dots & 0 \\ 0 & q_{22} & \dots & 0 \\ \dots & \dots & \dots & \dots \\ 0 & 0 & \dots & q_{nn} \end{bmatrix} \tag{29}$$

Lyapunov stability condition ($\dot{V} < 0$) is satisfied if the following condition is fulfilled:

$$2x^T Pu + \sum_{i=1}^{n+1} 2\lambda_i \gamma_i \dot{\gamma}_i \leq 0 \tag{30}$$

this last inequality is satisfied if $\dot{\gamma}_i$ are chosen in the following form:

$$\begin{aligned} \dot{\gamma}_1 &= \frac{1}{\lambda_1}(p_{n1}x_1 + p_{n2}x_2 + \cdots + p_{nn}x_n)y \\ \dot{\gamma}_2 &= \frac{1}{\lambda_2}(p_{n1}x_1 + p_{n2}x_2 + \cdots + p_{nn}x_n)y^{(1)} \\ \vdots &\quad \dots \qquad\qquad \dots \\ \dot{\gamma}_n &= \frac{1}{\lambda_n}(p_{n1}x_1 + p_{n2}x_2 + \cdots + p_{nn}x_n)y^{(n-1)} \\ \dot{\gamma}_{n+1} &= \frac{1}{\lambda_{n+1}}(p_{n1}x_1 + p_{n2}x_2 + \cdots + p_{nn}x_n)y_c(t) \end{aligned} \tag{31}$$

Considering (20) and (31) and $e^{(i)} = x_{i+1}$, the adjustment algorithm is deduced. The values p_{ni} are chosen based on the positivity conditions of the matrices P and Q.

$$\begin{aligned} \dot{k}_a(t) &= \frac{\sum_{i=1}^{n} p_{ni} e^{(i)}\, y_c}{k_0(T_k)\lambda_{n+1}} \\ \dot{c}_{n-1}(t) &= \frac{\sum_{i=1}^{n} p_{ni} e^{(i)}\, y^{i-1}}{k_0(T_k)\lambda_i} \end{aligned} \tag{32}$$

The control system is illustrated in **Error! Reference source not found.**. $\tau, \lambda_{1,2}$ and Q are carefully tuned to balance the competing objectives of tracking and disturbance rejection, see Table 6.

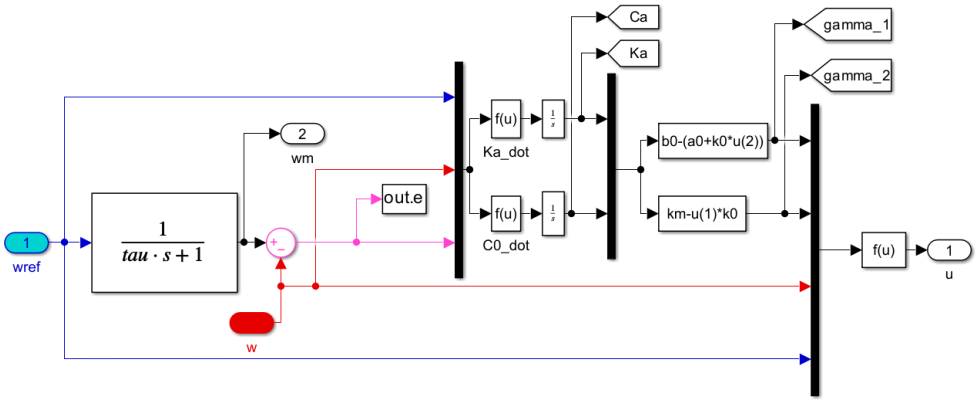

Fig9 Lyapunov-based MRAC block diagram.

Table 6 Lyapunov-based MRAC parameters

τ	$5 \cdot 10^{-5} s$
λ_1	0.1
λ_2	0.1
Q	0.001

The graphical outputs of the speed actuator (DC Motor) are plotted in Fig10, where the reference input for the angular velocity (a sinusoidal profile in this case) is compared to the reference model output and the actual output. As can be seen, the actual velocity successfully tracks

the reference velocity. This latter performs a high degree of alignment with the model reference output, demonstrating the effectiveness of the proposed adaptive control mechanism.

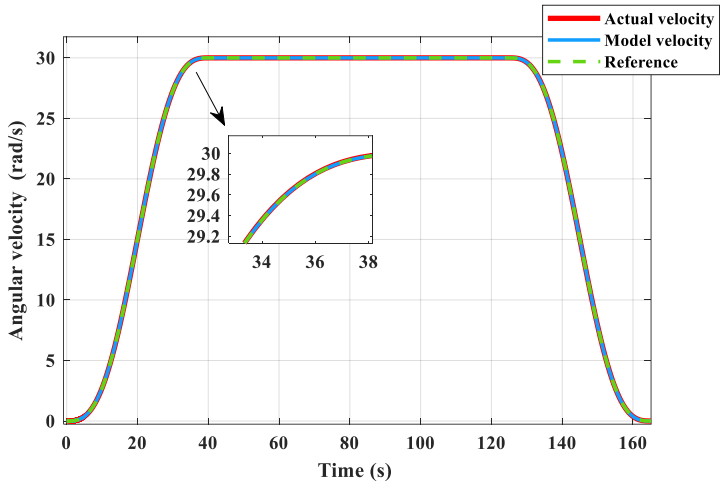

Fig10 Lyapunov-based MRAC angular speed results

VI. RESULTS AND DISCUSSION

To illustrate the effectiveness of the proposed control scheme, two tests are conducted on the overall system under various operating conditions. The chosen simulation scenario is a road segment of length $D = 2km$, the system conditions are given in Table 7.

Table 7 System parameters

Parameter	Wheel base L	Tire radius R	Speed limit V_m	Acceleration limit A_m
Value	2.96 m	0.2667 m	$8m/s$	0.4 m/s^2

A. Parametric Uncertainty Test

To assess robustness against parameter variation, Armature resistance R_a is increased by 200% while keeping all other parameters at their nominal values. The speed response before and after this variation is presented in Fig11. As expected, the conventional PID controller exhibits a noticeable delay after the resistance variation, with the tracking response deviating by approximately **0.1** seconds. Meanwhile, the GA-PID controller demonstrates improved performance, yet it still exhibits a deviation of about **0.05** seconds after the resistance change. In contrast, the MRAC controller maintains an unchanged response, its speed trajectory remains superimposed on the reference signal before and after the variation. Fig12 depicts the speed error plot, further illustrating the effect of the variation on controller performance. The conventional PID controller shows a relative increase of approximately 33.3%. Similarly, the GA-PID controller's overshoot rises from 0.007 to 0.009, corresponding to an increase of about 28.6%. In contrast, the MRAC controller maintains consistent performance with negligible change in error, confirming its superior ability to adapt and reject internal variations. Fig 13 illustrates the evolution of the Lyapunov-based MRAC adaptive parameters during resistance variation. The parameters adjust smoothly over time demonstrating the stability and effectiveness of the adaptation mechanism.

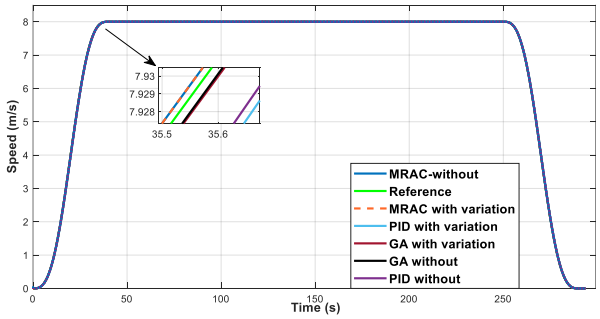

Fig11 Vehicle speed response with nominal and increased resistance.

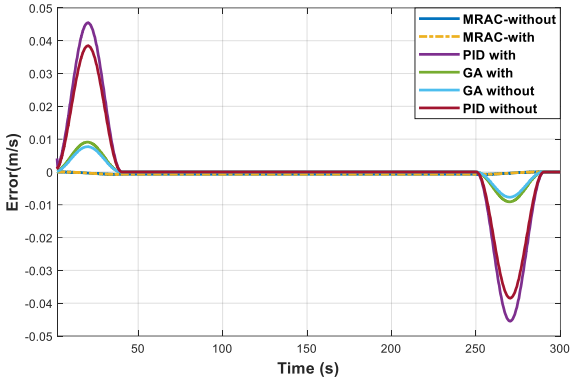

Fig12 Speed tracking error plot

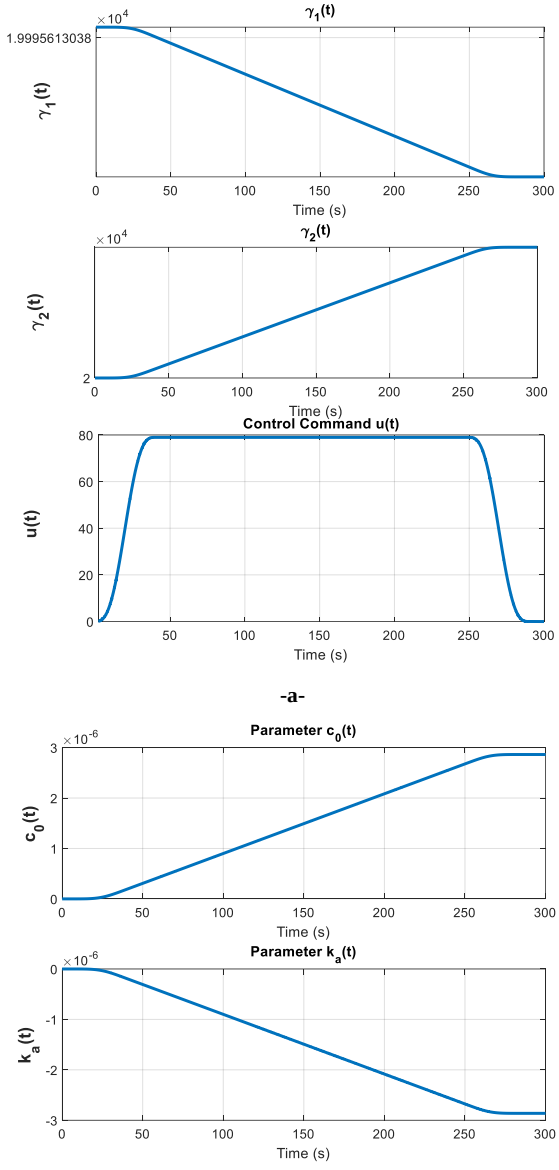

-a-

-b-

Fig13 Adaptive parameter evolution

B. Disturbance Rejection Test

In this test, the system is subjected to an external load disturbance. The load torque is initially set to its nominal value, 430 **N.m**, then increased by **10%** at time $t_1 = 50s$, and returns to nominal at $t_2 = 100s$.

Fig14 illustrates the speed plots of the three controllers. The conventional PID controller shows visible overshoot during the disturbance. The GA-PID controller demonstrates partial improvement but still exhibits a noticeable overshoot during the disturbance interval. In contrast, the MRAC controller maintains a consistent and accurate speed trajectory throughout the entire test.

Fig15 plots the corresponding speed error for all controllers during the load variation. The application of a 10% increase in load torque results in noticeable overshoots for the conventional PID and GA-PID of approximately **20%** and **15%** respectively. Both controllers exhibit a delayed recovery following the disturbance, indicating limited disturbance rejection capability. In contrast, the MRAC controller demonstrates high performance with a minimal hiccup of only **1%** and an instantaneous return to the reference trajectory.

Fig16 shows the evolution of Lyapunov-MRAC's adaptive parameters during the test. It is observed that the control law actively adjusts its adaptive parameters to produce a response that is insensitive to external disturbance.

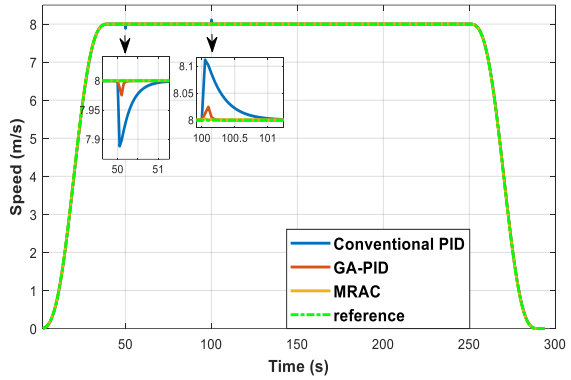

Fig14 Vehicle speed response after load disturbance.

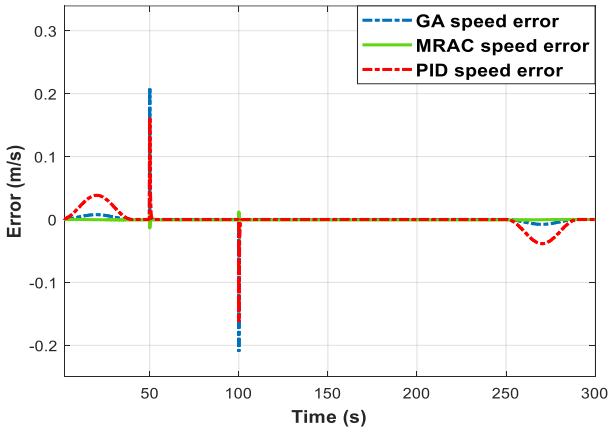

Fig15 Speed tracking error plot

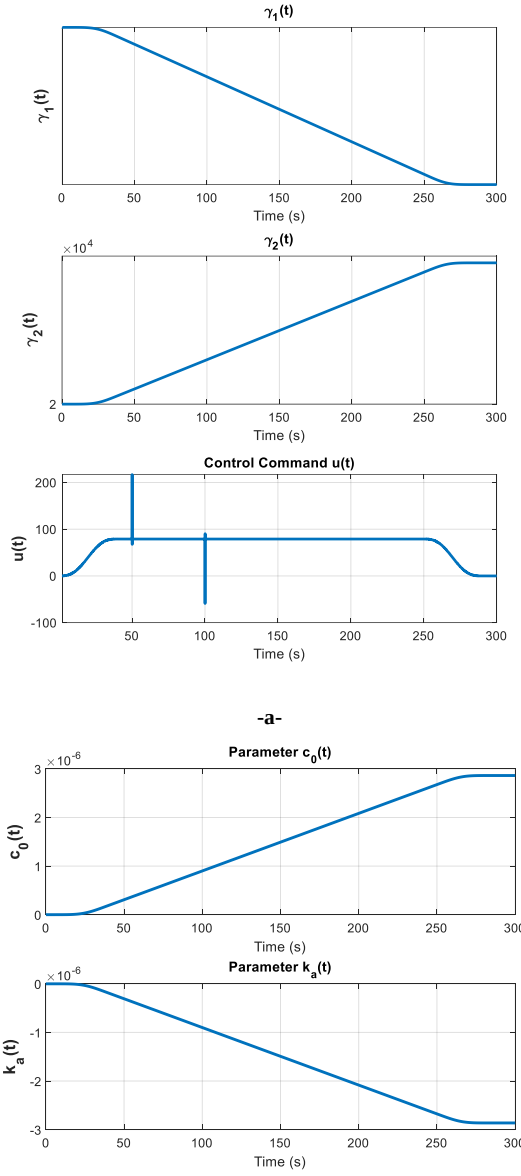

-a-

-b-

Fig16 Adaptive parameter evolution

VII. CONCLUSION

A modeling and simulation approach for Autonomous vehicles longitudinal control has been developed and introduced. Firstly, Sinusoidal and S-curve profiles were proposed to simulate realistic driving scenarios more accurately, leading a comparative study between the profiles, aiming to improve passenger comfort and safety. A classical PID controller was initially implemented for speed control. Although it performed adequately, it fell short in terms of accuracy. To enhance performance, a Genetic Algorithm (GA) was applied to optimize the PID gains, resulting in better performance. However, under dynamic uncertainties and parameter variations, a fixed configuration controller stays limited, which established the need for an adaptive control approach. Lyapunov-based model reference control was chosen for its ability to adjust controller parameters in real time, offering a more effective solution for handling uncertainties and ensuring reliable performance. Finally, simulation results were conducted under real-word conditions, demonstrating the effectiveness of the proposed adaptive mechanism. In conclusion, while the GA-optimized PID controller adapts well in ideal conditions, real-life variations and disturbances highlight the need for a more robust adaptive control strategy. Further work should be considered, such as implementing on-site scenarios to validate simulation results, and developing an extension of the proposed adaptive mechanism to more general systems.

ACKNOWLEDGMENT

The authors gratefully acknowledge the Engineering Systems, Design and Innovation (ESDI) group at the University of Bristol, UK (https://esdi.ac.uk/) for their support and the resources provided for this research.

REFERENCES

[1] Stamadianos, T., Kyriakakis, N. A., Marinaki, M., and Marinakis, Y., "Routing Problems with Electric and Autonomous Vehicles: Review and Potential for Future Research," *SN Operations Research Forum*, vol. 4, no. 2, 2023, Art. no. 00228. **doi: 10.1007/s43069-023-00228-1.**

[2] S. Cheng, L. Li, X. Chen, J. Wu and H. -d. Wang, "Model-Predictive-Control-Based Path Tracking Controller of Autonomous Vehicle Considering Parametric Uncertainties and Velocity-Varying," in *IEEE Transactions on Industrial Electronics*, vol. 68, no. 9, 2021. **doi:10.1109/TIE.2020.3009585.**

[3] Yeong, D.J., et al., "Sensor and sensor fusion technology in autonomous vehicles: A review," *Sensors*, vol. 21, no. 6, 2021, art. 2140. **doi: 10.3390/s21062140.**

[4] A. Artuñedo, J. Villagra and J. Godoy, "Jerk-Limited Time-Optimal Speed Planning for Arbitrary Paths," in *IEEE Transactions on Intelligent Transportation Systems*, vol. 23, no. 7, pp. 8194-8208, July 2022.**doi: 10.1109/TITS.2021.3076813.**

[5] Arevalo, V.M., Opticos, A., Ensenada, B.C., "Sinusoidal velocity profiles for motion control," *Proc. ASPE Control of Precision Systems*, Philadelphia, PA, USA, 2001, pp. 18–20.

[6] T. Alam, S. Qamar, A. Dixit, and M. Benaida, "Genetic algorithm: Reviews, implementations, and applications," *Int. J. Eng. Pedagog*., vol. 10, no. 6, pp. 57–66, 2020, **doi: 10.3991/ijep.v10i6.14567.**

[7] R. Ardhi, M. R. Febsya, A. Widyotriatmo and Y. Y. Nazaruddin, "Backward Motion Path Following Control of Autonomous Truck-Trailer: Lyapunov Stability Approach," *2019 IEEE Conference on Control Technology and Applications (CCTA)*, Hong Kong, China, 2019, pp. 900-905, **doi: 10.1109/CCTA.2019.8920669**.

[8] Lu, Y., et al., "A real-time decoupling trajectory planning method for on-road autonomous driving," *IET Control Theory & Applications*, vol. 17, no. 13, 2023, pp. 1800–1812. **doi:10.1049/cth2.12397.**

[9] A. Bou Ghosn, P. Polack, and A. de La Fortelle, "The Hybrid Extended Bicycle: A Simple Model for High Dynamic Vehicle Trajectory Planning," *arXiv preprint arXiv:2306.04857*, Jun. 2023. doi: 10.48550/arxiv.2306.04857.

[10] Rajamani, R., "Fundamentals of Vehicle Dynamics," SAE International, 2021.**doi: 10.4271/R-114.**

[11] L EROY-SOMER.(2020).D.C. motors 2 to 750 kW

[Online]. Available: https://www.leroysomer.com/documentation_pdf/3805_en.pdf.

[12] A. Lambora, K. Gupta and K. Chopra, "Genetic Algorithm- A Literature Review," 2019 International Conference on Machine Learning, Big Data, Cloud and Parallel Computing (COMITCon), Faridabad, India, 2019, pp. 380-384, **doi: 10.1109/COMITCon.2019.8862255.**

[13] Rothe, J., et al., "A modified model reference adaptive controller (M-MRAC) using an updated MIT-rule for the altitude of a UAV," *Electronics*, vol.9,no.7,2020,Art.no.1104.**doi:10.3390/electronics9071104.**

[14] Zelmat, M., "Automation of industrial processes Volume 2, Modal and adaptive control," Press Office of University Publications, 2001.

[15] A. Guendouz and A. Bouhenna, " Hyperstability criterion in model reference adaptive control: Enhancing induction motor efficiency for autonomous electric vehicles ", in *IoT-Enabled Energy Efficiency Assessment of Renewable Energy Systems and Micro-grids in Smart Cities*, M. Hatti, Ed. Cham: Springer Nature Switzerland, 2024, pp. 231–242. **doi: 10.1007/978-3-031-60629-8_24.**